Tuijin Jishu/Journal of Propulsion Technology
ISSN: 1001-4055
Vol. 45 No. 1 (2024)

Investigating Asia's Low-Latitude Ionosphere's Pulse During the Spectacular September 2017 Solar Storms

Ashish Kumar Meena[1], Preetam Singh Gour[2]
[1]*Ph.D. Scholar, Department of Physics, Jaipur National University, Jaipur, India*
[2]*Associate Professor, Department of Physics, Jaipur National University, Jaipur, India*

***Abstract*: -** This research examines fluctuations in Total Electron Content (TEC) variations in the ionosphere along the Asian longitude, focusing on the impact pertaining to solar flares and geomagnetic storms that occurred from September 6 to 9, 2017, in the geographical regions of India, Beijing, Dhaka, Islamabad, Thimphu, and Kathmandu. The investigation explores the impacts of solar flares in isolation and the compounded impact when both solar flares and geomagnetic storms coincide. On 6 September, two noteworthy X-class solar flares, specifically X2.2 at 08:57 UT and X9.3 at 11:53 UT, were observed during a period of calm geomagnetic conditions. The extreme ultraviolet (EUV)/X-ray intensity associated with the X9.3 flare was documented., with both flares exhibiting a slower recovery phase compared to their impulsive phase. This decelerated recovery in extreme ultraviolet (EUV)/X-ray intensity manifests as a delayed Total Electron Content (TEC) reaction. The observation of nearly an 10% greater crest-to-trough TEC variation on the day of the flare compared to the day before the flare indicates an intensified equatorial electrojet. The relatively subdued Total Electron Content (TEC) response to the X9.3 solar flare is ascribed to the shift in solar flare occurring from the disk centre towards the west limb. The solar flares on September 7-8 aligned with geomagnetic storms, leading to substantial TEC increments. These observed changes are attributed not only to the solar flares but also to the rapid penetration electric field and an elevated extent of thermosphere compositional alterations. On 9 September, 10 September, an escalation in the TEC was observed in solar flares of the M class under the joint influence of solar flares and a destroyed Dynamo electric field.

Key Word: *Solar flare (SF), Total Electron Content (TEC), X-ray, Extreme Ultraviolet (EUV), Geomagnetic storm.*

1. Introduction

Solar flares lead to a significant surge in solar irradiance, marked by a substantial increase of approximately 10 to 100 times in Soft X-rays within the range of 0.1 to 10 nm and around 2 to 10 times in extreme ultraviolet (EUV, 10 to 121.6 nm) radiation intensities. These escalations typically reach their peak within a short span of 10 to 30 minutes. The heightened irradiance in the soft X-ray and extreme ultraviolet (EUV) ranges swiftly elevate ionization levels in the upper atmosphere, causing perturbations in the ionospheric system. This, in turn, has repercussions on various technological systems, including wireless communication, the worldwide positioning system (GPS), and the trajectories of satellites. For instance, references such as Mitra (1974), Tsurutani et al. (2005), Liu et al. (2006), Coster and Komjathy (2008), and Qian et al. (2011, 2012a). Previous research has demonstrated that the impact of solar flares (SF) on the ionosphere system is contingent upon the location of the flares located on the solar disk [e.g., Zhang et al., 2002; Qian et al., 2010], as well as specific flare characteristics such as rise and decay times [e.g., Qian et al., 2011]. Moreover, solar flares (SF) can manifest either before or during the primary stages of geomagnetic storms, and also in the recovery phases of these storms. In these

situations, the intricate interaction between solar flares (SF) and geomagnetic storms adds an extra layer of complexity to the response of the ionospheric system to these concurrent events [e.g., Qian et al., 2012b].

The timeframe spanning from 6 September, 2017, to September 11, 2017, witnessed heightened space weather activity characterized by numerous solar flares and a pair of geomagnetic storms (see Figure 3,4). All these bursts of solar activity and storms emanated from a singular active region labelled #2673. Notably, the two most substantial flares, occurring on September 6 and September 10, 2017, were identified as a disk flare and a limb flare, each with comparable magnitudes. Specifically, The X9.3 flare that occurred on September 6, 2017, was categorized as a disk flare, while the X8.2 flare observed on September 10, 2017, manifested as a limb flare. Furthermore, a significant geomagnetic storm unfolded on 7 September, coinciding accompanied by a minimal southward component (Bz) of the Interplanetary Magnetic Field at approximately -30 nT (refer to Figure 3,4). Following this event, a smaller storm occurred on September 8, linked to a minimal southward IMF Bz value of about -18 nT (Figure 3,4). This space weather occurrences present a valuable an opportunity to study the impacts of solar flares on the ionosphere system and explore the intricate interplay among the impacts of solar flares and geomagnetic activity. For instance, the study by Bagiya et al. [2018] delved into the ionospheric Analysing the reactions to the concurrent effects of solar flares and a geomagnetic storm from 6 to 8 September, 2017, with a focus on Asia's Low-Latitude.

The position of a solar eruption on the Sun plays a crucial role in shaping the behaviour of the ionosphere system to the solar eruption. While the enhancement of soft X-rays remains largely unaffected by the flare's location, the increase in Extreme Ultraviolet (EUV) radiation resulting from a disk flare is significantly greater than that from a solar eruption occurring on the limb of equivalent intensity, particularly in various wavelengths exceedingly approximately 30 nm. This pronounced EUV enhancement for a disk flare arises from the differing opacity of soft X-rays and extreme ultraviolet (EUV) in the solar atmosphere.

Which dominate the spectrum of soft X-rays, are typically transparent in the solar atmosphere. Consequently, the absorption of gentle X-rays as they traverse the solar atmosphere experiences minimal variation with the location of the flare, whether it's at the center or the limb. In contrast, chromosphere Emissions that predominate in the EUV spectrum are frequently optically dense in the solar atmosphere. The absorption of such dense emissions is more substantial when a solar flare occurs at the limb because of the increased optical path length. As a result, limb flares exhibit reduced enhancement in EUV wavelengths. Former investigations explored the positioning of a solar flare influenced Ionospheric responses. Nonetheless, these investigations were either statistical analysis correlating location-based impacts with ionosphere responses [Zhang et al., 2002] or simulations using numerical methods utilizing presumed and idealized solar flare scenarios [Qian et al., 2010]. These studies were unable to scrutinize a pair of solar flares identical of comparable magnitude originating originating from the same active region, yet differing as flares occurring on the solar disk compared to those on the solar limb. when observed from Earth. The occurrence of the X9.3 solar disk flare and the X8.2 solar limb flare, both emerging from the same region, provides a unique opportunity to investigate the actual ionosphere system reactions to these solar flares.

Qian et al. [2012b] undertook modeling studies to investigate the impact of an X1.7 solar flare affecting large-scale Traveling Atmospheric Disturbances (TADs). This particular X1.7 flare took place on October 28, 2003, coinciding with the recuperation stage of a moderate geomagnetic storm occurring on the same day. The study revealed that the flare induced a robust specific increase in Joule heating. This, combined with pre-existing expansive traveling atmospheric disturbances (TADs) initiated by the storm before the solar flare, resulted in heightened traveling atmospheric disturbances (TADs). These disturbances conveyed transferring energy and momentum towards the equatorial region as they moved toward the equator. Conversely, simulated models suggested that, assuming geomagnetically tranquil circumstances, substantial Joule heating concentrated in a specific area and large-scale atmospheric disturbances TADs did not occur during the solar flare. This numerical investigation suggested that solar flares by themselves were insufficient to trigger expansive traveling atmospheric disturbances (TADs). During the period from September 6 to September 11, 2017, most flares transpired amid geomagnetically quiet conditions, notwithstanding geomagnetic storms on September 7 and September 8, 2017. The storm that occurred on September 7 happened subsequent to an X1.3 flare on the same day, along with several M class flares coincided in conjunction with the storms over these two days (Figure 3,4). In contrast to the October 28, 2003 event scrutinized by Qian et al. [2012b], which featured the simultaneous existence of a X1.7 solar flare

and geomagnetic storms during the September 2017 timeframe offers a chance to investigate occurrences involving extensive-scale TADs in distinct circumstances. These conditions include the simultaneous occurrence of solar flares and geomagnetic storms and scenarios involving solar flares lacking accompanying geomagnetic storms.

This document employs models simulated scenarios and analyzing data for the specified duration until explore the Ionosphere reactions to solar flares. The emphasis is on comprehending ionosphere reactions to the X9.3 solar disk flare and X8.2 solar limb flare, considering the effects of flare's position. Additionally, the study investigates the incidence involving extensive-scale TADs stemming from geomagnetic storms and solar flares.

2. Data Set

You can obtain the X-ray data averaged over one minute (0.1–0.8 nm) from the following URL: http://www.swpc.noaa.gov/products/goes-x-ray-flux. The 15-second EUV flux data (24–34 nm) averaged over a specific period can be acquired from this URL: https://dornsifecms.usc.edu/space-sciences-center/download-sem-data/. For information on geomagnetic conditions amidst a solar flare event, you can refer to the Dst index, the north–south component of the Kp, interplanetary magnetic field (IMF Bz) indices. These indices are available through the Data Centre, (http://wdc.kugi.kyoto-u.ac.jp), and the Omni web website (https://omniweb.gsfc.nasa.gov).

The International Reference Ionosphere (IRI) is a widely recognized and utilized model for the Earth's ionosphere. It provides valuable information, including Total Electron Content (TEC) data. TEC is a gauge of the quantity of electrons within a unit cross-sectional area column extending from the Earth's surface to the upper part of the ionosphere. IRI TEC data is crucial for various applications, such as global navigation satellite systems (GNSS), including Global Positioning System (GPS). Users in fields like telecommunications, satellite communications, and space weather monitoring rely on IRI TEC data to understand and predict variations in the ionospheric electron density. To access IRI TEC data, you can refer to official sources such as the Center for Space Science and Radio Engineering (CSSRE) at the National Technical University of Ukraine "Igor Sikorsky Kyiv Polytechnic Institute," which plays a role in maintaining and updating the IRI model. The International Reference Ionosphere (IRI) model provides a representation of the Earth's ionosphere, including the Total Electron Content (TEC). The mathematical equations used in the IRI model are complex and involve various parameters to describe the electron density at different altitudes and geographic locations. The model employs empirical formulations based on a vast array of ionospheric observations.

One commonly used formula to calculate TEC in the IRI model is as follows:

$$TEC = \int_{h1}^{h2} \mathrm{ne}(h)dh$$

Where:

- TEC stands for Total Electron Content.
- $n_e(h)$ represent the electron density at altitude.
- dh is an infinitesimally small change in altitude.
- h_1 and h_2 are the lower and upper limits of the integration, typically representing the altitudes from the bottom to the top of the ionosphere.

The electron density Ne(h) is modeled using a combination of functions and parameters, and the IRI model has different formulations for different ionospheric regions (e.g., F1, F2 layers). The exact equations used by the IRI model can be quite involved and depend on the specific region, time of day, and geographic location.

3. Results

On September 3, 2017, the sunspot group located within the active region labeled as #2673, situated at S10W30 (as shown in Fig. 1), underwent a remarkable expansion, growing fourfold within a single day (source: www.spaceweather.com).

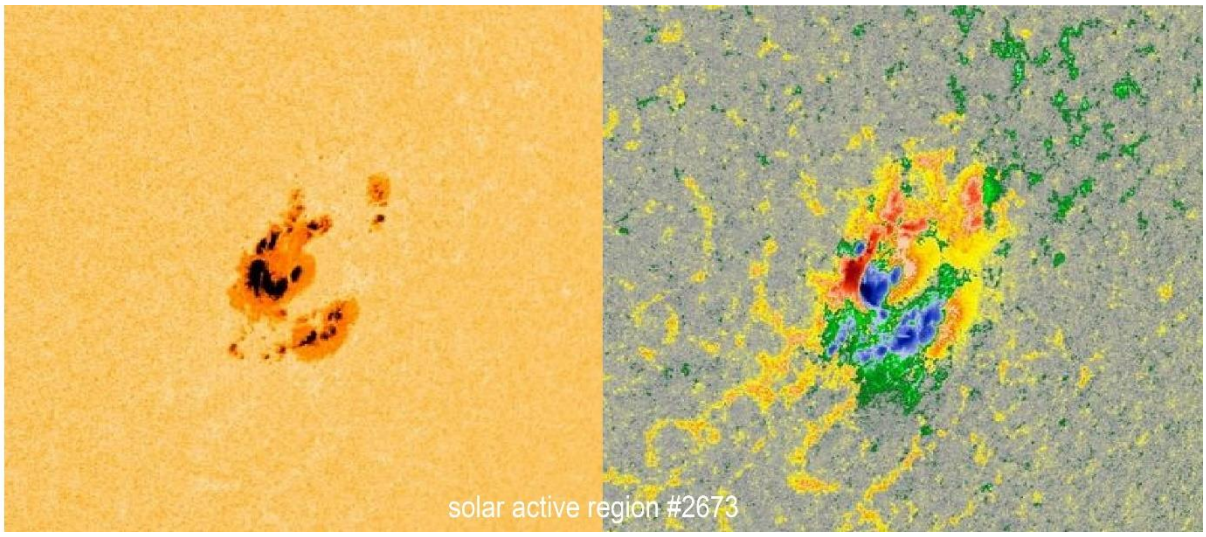

Figure 1: The solar active region designated as #2673 generated multiple solar flares from September 6 to 10, 2017.

The progression in the number of sunspots correlates with an increased instability in the magnetic field. The rapidly developing active region #2673 exhibited a 'beta-gamma' magnetic field, culminating in the release of an M5.5 flare at 20:33 UT on 4 September, 2017. Following days witnessed a succession of solar flares impacting the Earth atmosphere. The shifting position of the solar active region from September 6 to 10 is observable in Figure 1 and 2. Specifically, the active solar region 2673 position on September 6 indicated disk flares, with rotation towards the west limb.

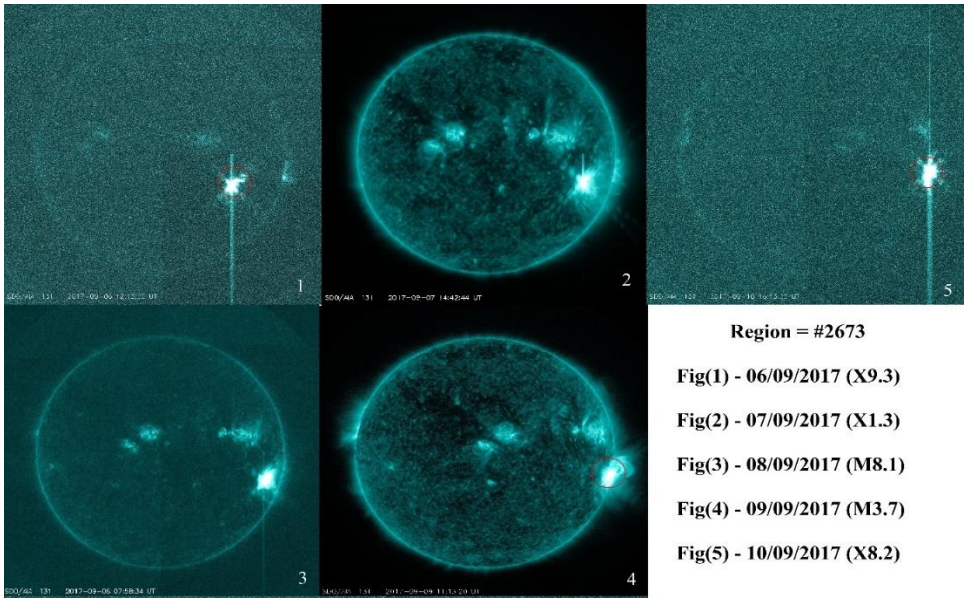

Figure 2: Depicts a magnetogram illustrating the position of the solar active region #2673, which generated multiple solar flares between September 6 to 10, 2017.

The Earth experienced the impact of the X9.3 flare on 8 September 2017. To assess the ionospheric reaction throughout the events spanning September 6 to 10, 2017 we analyzed Total Electron Content (TEC) data from selected locations in East and South Asia. The chosen capitals for this investigation included Delhi (28.7041°N, 77.1025°E), Beijing (39.90°N, 116.40°E), Islamabad (33.68°N, 73.04°E), and Dhaka (23.80°N, 90.41°E). Additionally, the high latitude capitals Thimphu (27.47°N, 89.63°E) and Kathmandu (27.71°N, 85.32°E) were incorporated into the analysis to provide a thorough comprehension of the ionospheric impacts.

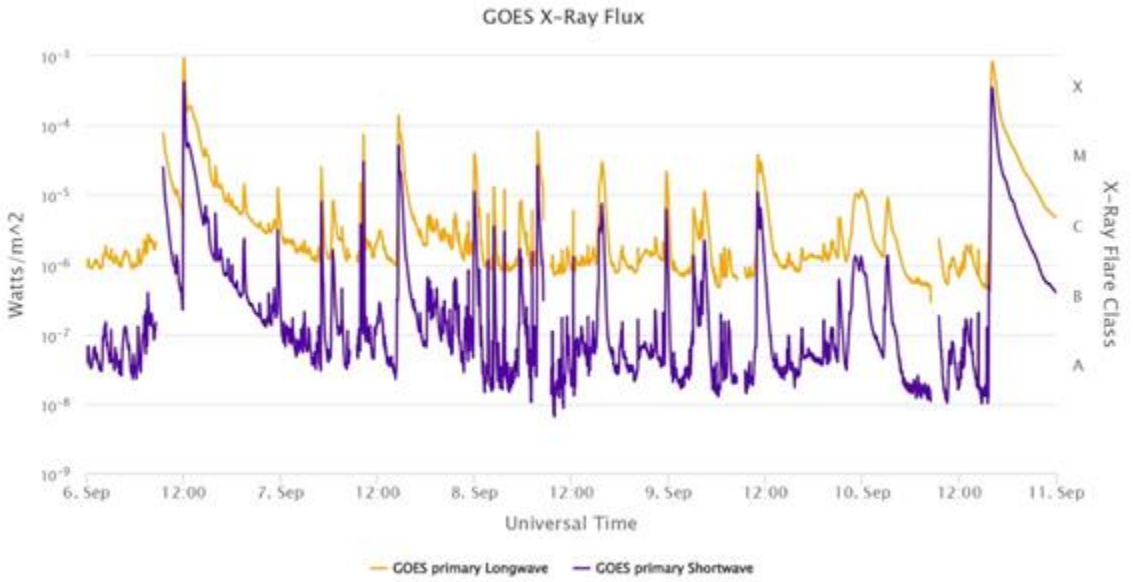

Figure 3: The variability in X-ray flux observed during the solar eruption spanning September 6 to September 10, 2017.

Figure 3 displays GOES the X-ray emissions within the wavelength range from 0.1 to 0.8 nm, as detected by the Geostationary Operational Environmental Satellite (GOES). The accompanying panels (figure 4A to figure 4D) illustrate the Interplanetary Magnetic Field (IMF) components By (figure 4A) and Bz (figure 4B) obtained retrieved from the Omni database, the Disturbance Storm Time (Dst) index (figure 4D), and the Planetary Index Kp (figure 4C). The data spans from September 6 to September 10, 2017. The empirical model of auroral electric potential proposed by Heelis, as delineated by Heelis et al. (1982). Notably, this model utilizes the Planetary Index Kp as a crucial parameter. Solar flares undergo classification based on The classification is based on their X-ray peak flux within the 0.1 to 0.8 nm wavelength range, expressed in Watts per square meter (W/m^2). The classification includes three categories: X-class, M-class, and C-class, each corresponding to peak X-ray fluxes falling within The intervals $I > 10^{-4}$, $10^{-5} \leq I < 10^{-4}$, and $10^{-6} \leq I < 10^{-5}$ delineate these ranges, respectively.

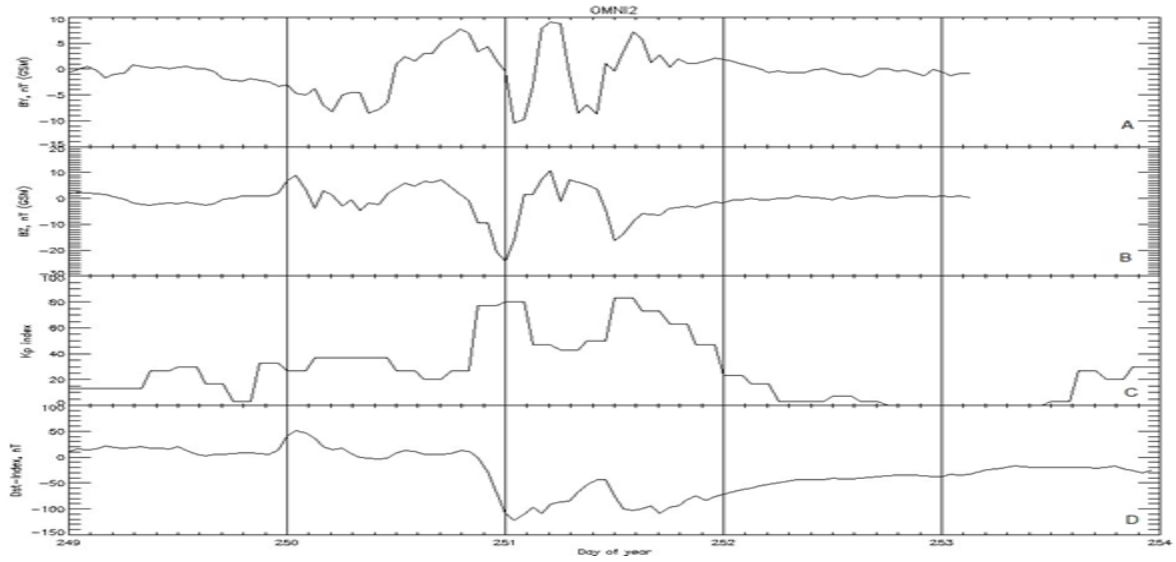

Figure 4: Displays data extracted from the Omni database, illustrating IMF By and Bz parameters alongside geomagnetic Kp and Dst indices covering the timeframe of September 6 to September 11, 2017. The panels present the following: (A) IMF By, (B) IMF Bz, (C) Kp, and (D) Dst.

As depicted in Figure 3, the solar activity during the specified timeframe exhibits numerous X class solar flares and a considerable quantity of M-class of flares. Additionally, C-class flares are observed consistently throughout this period. Notably, a significant geomagnetic storm transpired on 7 September 2017, characterized by a minimum Bz at approximately -20.6 nT and a minimum Dst index at around -68 nT. Yet another geomagnetic storm unfolded on 8 September, featuring a minimal Bz at roughly -24.2 nT and a minimum Dst at about -122 nT. The peak Kp values during these two storms reached a level of approximately 8. It's noteworthy that solar flares were present both before, during, and after these geomagnetic storms, indicating a dynamic interaction between solar activity and geomagnetic disturbances throughout this period.

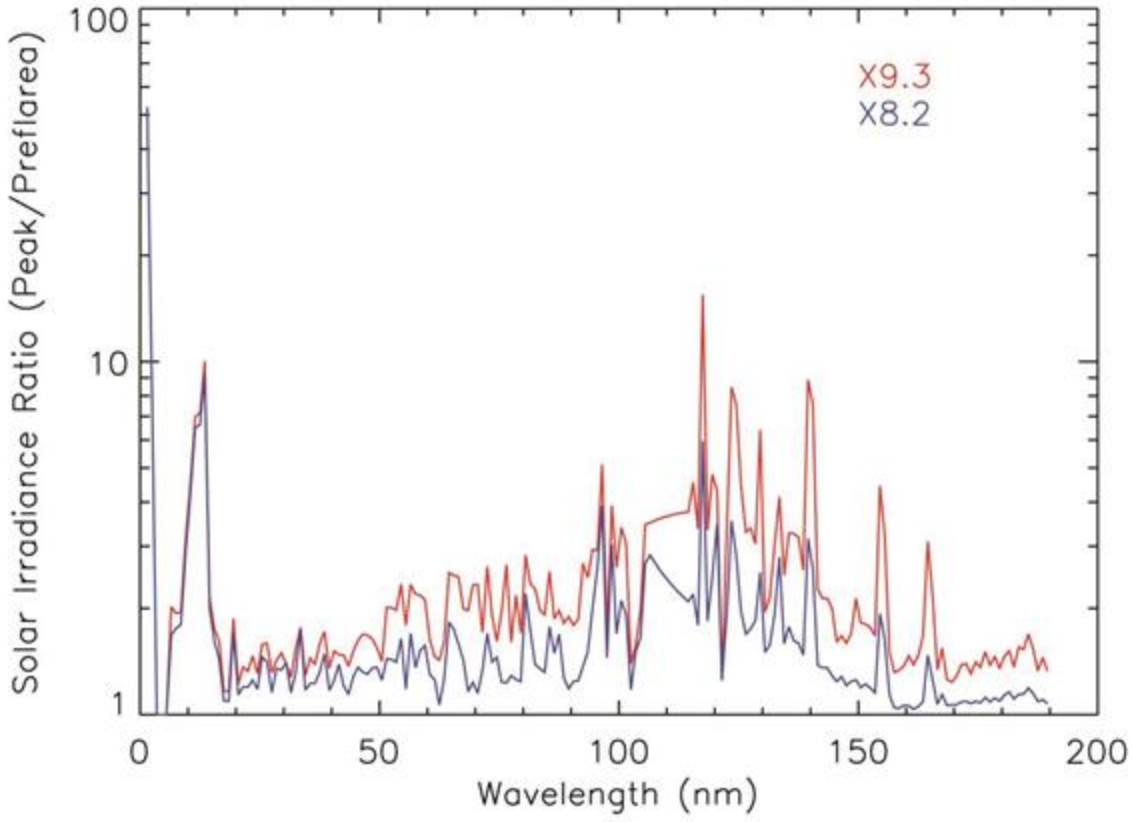

Figure 5: The comparison of solar irradiance ratios, specifically between the intensity at the peaks of flares and the pre-flare levels, is depicted in the following manner: The red curve represents the ratio pertaining to the X9.3 disk flare, while the blue curve represents the ratio for the X8.2 limb flare.

Figure 5 illustrates the solar irradiance ratio during the peak of the X9.3 disk flare and the X8.2 limb flare relative to their pre-flare levels, as computed by the Fast-Imaging Solar Spectrograph (FISM). The observation times for the X9.3 flare were at 11:52 UT before the flare and at 12:02 UT during the peak, while for the X8.2 flare, the corresponding times were 15:45 UT and 16:06 UT, respectively. Solar flares are typically categorized based on their peak solar flux in the wavelength range of 0.1 – 0.8 nm. Specifically, the maximum solar flux values for the X9.3 and X8.2 flares within this wavelength range were 9.3×10^{-4} W/m2 and 8.2×10^{-4} W/m2, respectively. Despite the similarity in the magnitudes of these flares, the solar irradiance increases for the X9.3 solar disk flare is solely marginally higher than that for the X8.2 solar limb flare in the wavelength range below 20 nm. In wavelengths beyond 20 nm, the variation in solar irradiance enhancement between the two flares is even smaller if their locations are the same. This is because solar irradiance enhancement typically diminishes with longer wavelengths.

Yet, in the wavelength range beyond 20 nm, the solar irradiance enhancement of the X9.3 solar disk flare significantly surpasses that of the X8.2 solar limb flare, as depicted in Figure 5. This discrepancy can be attributed to the distinct opacity of soft X-rays and extreme ultraviolet radiation in the atmosphere of the Sun, this leads to a disparity in the enhanced extreme ultraviolet (EUV) flux between the X9.3 and X8.2 solar flares is more pronounced than it would be were their locations were identical. These additional differences in EUV enhancement, stemming from the distinct locations of the flares, manifest within the Ionosphere reactions to these events. It is noteworthy that the X8.2 solar flare, initially classified as an over the limb solar flare, implies many emissions from the optically thick chromospheric and transition regions, particularly those exceeding 20 nm, were initially obscured by utilizing the solar disk. This resulted in a more substantial reduction compared to the variability in emissions from the center to the limb. However, as the flare progressed, a footprint-like flare ribbon extended over the limb flare, leading to an augmentation of these emissions (Chamberlin et al., 2018). For simplicity, the referenced paper refers to this event as the X8.2 limb solar flare.

Given that soft X-rays predominantly influence ionization within the E-region, while Extreme Ultraviolet (EUV) radiation predominates in ionization above approximately 160 kilometer altitude (Qian et al., 2010), the expectation is that the positioning of a solar flare impact Ionosphere responses above ~150 km but not within the E-region. To scrutinize these flare location effects, data and model simulations are employed in the examination of ionosphere responses to the X9.3 solar disk flare and the X8.2 solar limb flare.

6 September 2017, incident

On September 6, solar activity in the form of a pair of X-class solar flares occurred, specifically X2.2 at 08:57 UT and X9.3 at 11:53 UT, emanating from the solar active region 2673's occurrences. The X2.2 solar flare reached its peak at 09:10 UT and commenced its decay around 09:17 UT. Subsequently, the X9.3-class solar flare reached its peak at 12:02 UT and underwent decay by 12:10 UT. The relative strength of these solar flares is shown in Fig. 3. The ratio for The X9.3 flare's relative intensity was 1.67/6.00 times greater than that of the X2.2 flare. Of note, the recovery phase of both solar flares was observed to be slower compared to their respective impulsive phases, with the intensity of EUV declining slightly more gradually than that of X-rays. Geomagnetic activity on September 6, as indicated by Fig. 3, did not exhibit any disturbances.

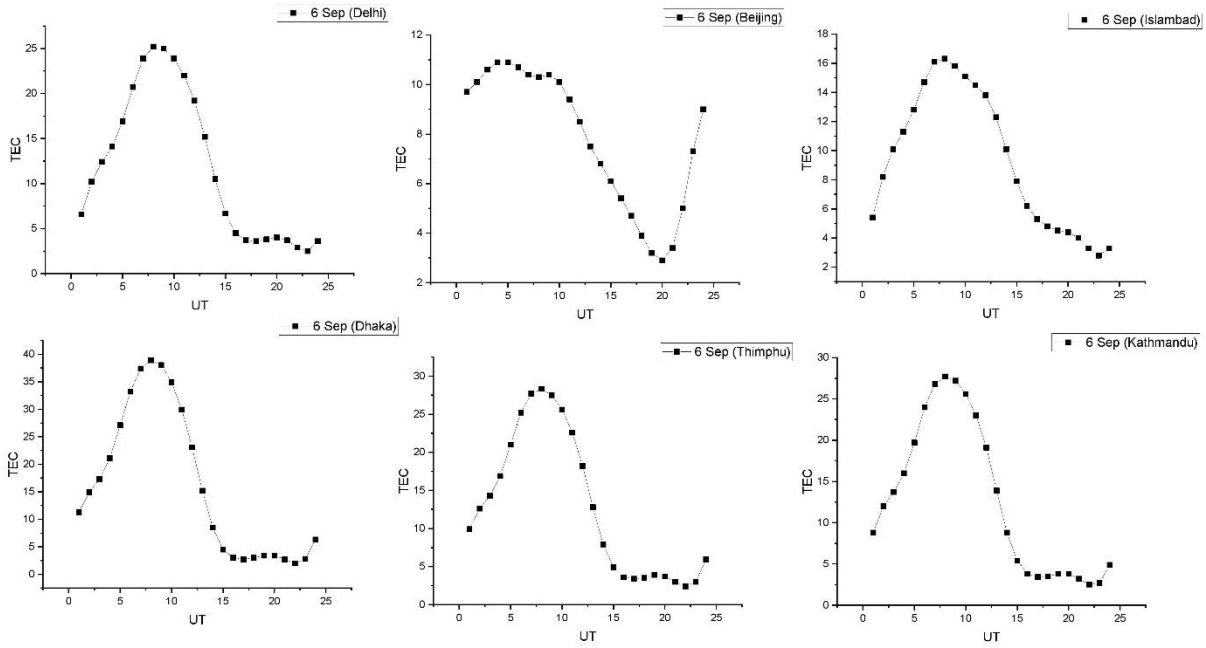

Figure 6: The TEC variation diurnal pattern during the solar flare events on September 6, 2017, is illustrated. On that particular day, the X2.2 solar flare took place at 08:57 UT, followed by the X9.3 flare at 11:53 UT.

The Dst index surpassed -30 nT, and the Planetary index remained below 4. IMF Bz began fluctuating at 23:53 UT. The preceding morning of September 6 was magnetically quiet, characterized as indicated by 3-hourly

planetary Kp indices of 1, 1, 1, 3, 3, 2, 0, 3. From figure 6 shows the diurnal variation of total electron content (TEC) on September 6, 2017, in Delhi, Beijing, Islamabad, Dhaka, Thimphu, and Kathmandu. TEC values are provided at hourly intervals along with the given exact occurrence times of various solar flares (SF) that day. The most significant solar flares were an The X2.2 flare, which occurred at 08:57 UT, reached its peak at 09:10 UT, while the X9.3 flare at 11:53 UT peaked at 12:02 UT. Analysis of the TEC values shows a clear diurnal pattern in all locations, with minimum values occurring in the early morning hours and maximum values in the afternoon. This is consistent with known ionospheric behavior due to photoionization from solar radiation. However, significant deviations from the smooth diurnal pattern are visible, especially during times of intense solar flares. The X2.2 solar flare appears to have caused an almost immediate increase in TEC, noticeable in all locations. In Delhi, TEC jumped from 14.1 to 16.9 between the hour before and after the flare onset. Even larger increases occurred in the equatorial locations like Dhaka and Islamabad, with TEC increasing by over 6 TEC units in Dhaka. This swift response indicates prompt penetration of solar flare-related disturbances into the ionosphere. The more intense A few hours later, the X9.3 solar flare triggered even greater TEC enhancements. In Delhi, the TEC rose from 16.9 just before the flare to 23.9 in the hour after, an increase of over 7 TEC units. Similar increases of 9-12 TEC units occurred in equatorial regions. However, the peak TEC value was reached 1 hour after the flare started in Delhi but showed a higher lag time of 2 hours in equatorial sites. This indicates the time taken for complete propagation of ionospheric disturbances from the sub-solar point.

The TEC enhancements due to both solar flares were short-lived, with TEC recovering back close to pre-flare levels 2 to 3 hours after flare onset. This is consistent with studies that have found solar flare impacts on the ionosphere, especially the equatorial ionosphere, tend to manifest and recover promptly. Besides the flare-induced TEC changes, other smaller-scale variations are also visible throughout the diurnal cycle. These could be caused by phenomena like equatorial plasma bubbles, sporadic E formations, or gravity waves that commonly affect ionospheric stability. Detailed modeling and analysis would be required to ascertain their exact causes. Overall, this TEC data provides solid evidence of prompt and significant Reaction of the low-latitude ionosphere to a powerful solar flare events. It is a prime example of space weather-driven disturbances in the upper atmosphere causing deviations from expected diurnal patterns. The data reinforces solar flares and activity as one of the key drivers of fluctuations in ionospheric total electron content. Capturing and modeling such data can improve understanding and predictions of the complex sun-earth interaction. In addition to longitudinal biases, the findings indicate that the latitudinal responses exhibited symmetry in Total Electron Content (TEC) concerning the X9.3 solar flare. The augmentation of TEC commenced diminishing alongside the diminishing of Extreme Ultraviolet (EUV) emission strength. Nevertheless, the TEC level persisted at an elevated state for approximately 3 hours before returning to the baseline level around 16:00 UT. The slower recovery time observed in the TEC trend can be ascribed to the gradual decline of EUV, in contrast to X-ray irradiance. Furthermore, our examination unveils a temporal time lag between the decline in EUV emission and the subsequent reduction in TEC. Clues regarding this time lag can potentially be gleaned from the recent study by Yasyukevich et al. (2018). According to their observations, Yasyukevich et al. noted a significant delay spanning several hours between the decline of Extreme Ultraviolet (EUV) emission and the recovery of Total Electron Content (TEC). They elucidated this temporal gap by referencing the work of Qian et al. (2011), who proposed that the extended diminishing of flare emission, coupled with substantial contributions from elevated altitudes, might account for the delayed return of TEC to its pre-flare baseline. Moreover, the intricate interplay of the thermosphere-ionospheric coupling, primarily perturbed by a solar flare, was identified as a potential factor causing a delay in the ionospheric response, as highlighted by Zhang et al. (2017). Further supporting this notion, Li et al. (2018) uncovered a 4–5-hour lag in TEC recovery to its baseline level during quiet times. In the 2019 study conducted by Qian et al. 2019, there is a suggestion that solar flares occurring above 150 km primarily influence the ionospheric response, with disk flares exerting a more substantial impact compared to limb flares. Moreover, this effect exhibits notable dependence on both local time and longitude positions.

September 7-8, 2017 incident-

On September 7 from Figure 7, solar activity was extremely high, with multiple M and X class flares originating from the active region 2673. The first notable event occurred at 04:59 UT – an M2.4 class solar flare, followed

by several other minor flares in quick succession. This led to discernible changes in TEC – in Delhi, the TEC increased from 14.2 before the flares to 17 within an hour, representing a ~3 TECU enhancement. The subsequent hours saw even greater changes; an M7.3 flare at 10:11 UT preceded drastic TEC rises of 6-8 TECU across all sites. The most intense flare was an X1.3 class event starting at 14:20 UT, resulting in prompt and dramatic TEC increases that constitute the main daytime peak. In Delhi, the TEC rose from 17 at 13:00 to 24 at 15:00 – a remarkable 7 TECU enhancement within two hours of the X1.3 flare onset. The subtropical site Beijing saw slightly more moderate TEC changes; however, equatorial locations like Dhaka and Islamabad registered >10 TECU rises within hours of the X1.3 event.

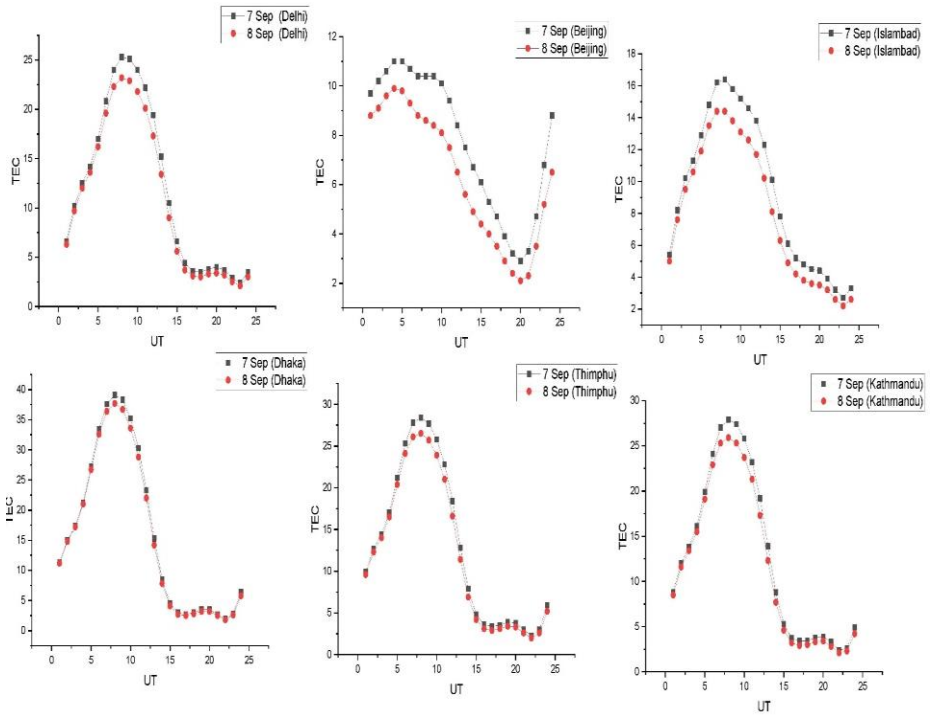

Figure 7: Illustrates the diurnal profile of TEC variation during September 7–8, 2017. On September 7, several M-class solar flares occurred, including M2.4 (04:59 UT), M1.4 (09:49 UT), M7.3 (10:11 UT), X1.3 (14:20 UT), and M3.9 (23:50 UT). On September 8, additional flares took place, namely M1.3 (02:19 UT), M8.1 (07:40 UT), M2.9 (15:09 UT), and M2.1 (23:33 UT).

Beyond the main flare period 14:20 – 14:55 UT, minor fluctuations notwithstanding, the enhanced TEC levels persisted for 3-4 hours before recovering close to the pre-flare state. This indicates a prolonged disturbance and recovery phase of the ionospheres in reaction to an intense X-class solar eruption. Moving to September 8, while several minor C-class flares occurred, the effects were not as distinctly observable in the TEC as the previous day's major events. However, three M-class solar flares occurred: the M1.3 flare at 02:19 UT, the M8.1 flare at 07:40 UT, and the M2.9 flare at 15:09 UT. registered clear TEC signatures. The TEC continued its decreasing night-time trend during the M1.3 event, but rise rapidly afterward leading to a slightly early morning enhancement in all sites. The M8.1 event caused pronounced TEC fluctuations during 07:00 – 09:00 UT, superimposed on the expected pre-noon increasing trend. Lastly, the M2.9 flare coincided exactly with the time of daily TEC peak in Delhi. The TEC maximized at 16:20 UT, suggesting a probable contribution from this flare-associated ionization. An important aspect is that throughout the two days, the diurnal patterns and ranges in equatorial locations were significantly greater relative to sub-tropical sites like Delhi and Beijing, clearly highlighting the difference in ionospheric characteristics across latitudes. The equatorial ionosphere namely over Dhaka and Islamabad also registered sharper hour-to-hour changes during flare events. This indicates flare-induced effects were manifested more prominently near the magnetic equator where the background ionosphere is already unstable.

Additionally, minor fluctuations, some seemingly unrelated to the solar flares were also seen occasionally. These could arise from other sources of disturbance such as sporadic E-layer formations, spread F irregularities, or traveling ionospheric disturbances propagating from auroral latitudes. While outside the present scope, further analysis through modeling and removing flare contributions can help isolate and study contributions from other geophysical phenomena affecting ionospheric stability.

Overall, these results demonstrate solar flares being a dominant space weather factor introducing major fluctuations in low latitude total electron content, especially under high solar activity conditions as the solar cycle enters its declining phase. The TEC over Delhi provides a good indicator for ionization trends over the Indian sub-tropical region. The data covers an excellent sequence of flares during September 7-8, 2017 illustrating prompt enhancements in TEC in reaction to M and X class solar flares eruptions. It highlights the time scales over which such disturbances manifest and subside in the upper atmosphere. From an application perspective, incorporating real-time flare monitoring and predicting resultant TEC fluctuations can improve the accuracy of HF communication and GNSS systems which are sensitive to the levels of electron density in the ionosphere. The present data and analysis provide useful insights for further studies exploring modeling, forecasting, and mitigating adverse space weather impacts on critical infrastructure across latitudes.

The event occurred on September 9-10, 2017

Figure 8 illustrates the daily variation of ionospheric total electron content (TEC) over six locations Delhi, Beijing, Islamabad, Dhaka, Thimphu, and Kathmandu on September 9–10, 2017. The figure highlights several M-class solar flare events on September 9, including an M3.7 flare at 10:50 UT and an M1.1 flare at 22:04 UT. September 10 saw an intense X8.2 flare at 15:35 UT, constituting one of the largest flares during Solar Cycle 24. The flare timings align with discernible perturbations in the TEC evolution, affirming significant ionospheric responses. On September 9 across all stations, the smooth pre-dawn increase gives way to a consistent morning enhancement that constitutes the primary daytime TEC peak, typically occurring between 10:00 to 11:00 UT. The sub-tropical sites Delhi and Beijing register lower overall TEC compared to the equatorial belt where values over Dhaka and Islamabad remain elevated throughout the day. This conforms to known latitudinal differences in ionization patterns. In Delhi, the noontime TEC peaks at 23.3 TECU while Dhaka registers a maximum of 37.7 TECU – over 60% higher, highlighting the Equatorial Ionization Anomaly (EIA) influence. The afternoon decay rates also differ – the TEC over equatorial locales decreases gradually indicating the persistence of additional ionization mechanisms like equatorial fountain effects. In contrast, the drops in sub-tropical locations are sharper as recombination processes dominate in the evening hours. These distinct trends repeating over days confirm typical ionospheric characteristics in the two regions.

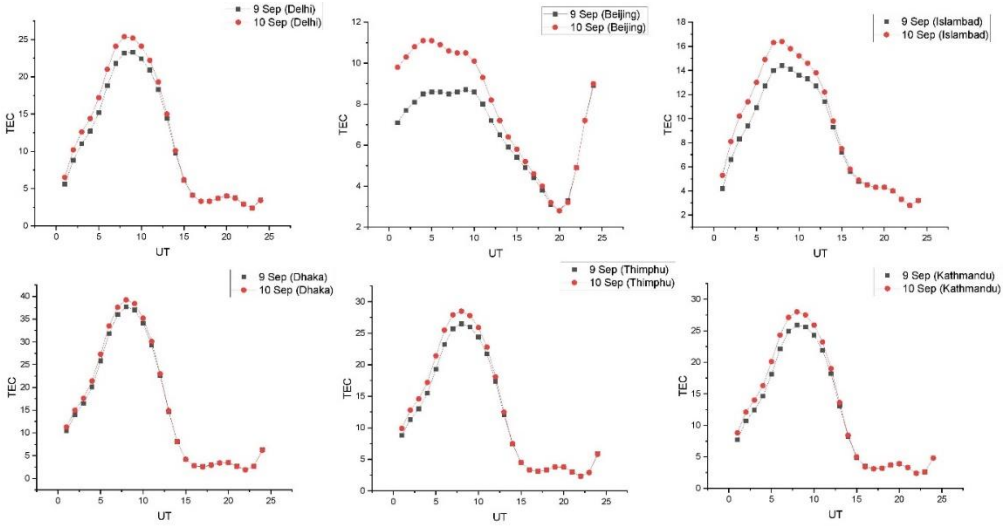

Figure 8: Displays the diurnal TEC variation profile on September 9-10, 2017. On September 9, several M-class solar flares, specifically M1.3 (03:09 UT), M1.1 (04:14 UT), M3.7 (10:50 UT), and M1.1 (22:04 UT), occurred. On September 8, additional flares took place, namely X8.2 (15:35 UT).

However, clear signatures of transient perturbations from the solar flare events are also evident. On September 9, the M3.7 flare onset at 10:50 UT occurred close to the background TEC peak time. An intensified rising trend is seen in the next 1-2 hours with the peak value advancing and exceeding quiet day levels across sites. This points to prompt penetration of solar flare-associated shock waves which enhance ionization. The TEC remains elevated for a longer duration before recovering gradually. The isolated nighttime M1.1 flare also potentially contributes to slight enhancements near local midnight compared to previous nights. The effects are even more prominently seen on September 10 following the exceptional X8.2 solar flare event. The enormous eruption beginning at 15:35 UT introduces major disturbances in the dayside ionosphere during local afternoon hours. In Delhi, the TEC nearly doubles from 14.4 at 15:00 UT to 24.1 at 17:00 UT representing an unprecedented ~10 TECU rise within two hours of the intense X-class flare. Similar extreme enhancements occur over equatorial sites albeit more gradually due to the added presence of other counteracting density gradients and electric fields. Nonetheless, in Dhaka, the TEC peaks at 37.6 TECU – among the highest values registered during September 2017, affirming significant supplements from this major solar eruption. The TEC takes nearly 6 hours across stations to recover close to quiet levels indicating an extended disturbance and recovery phase of the low-latitude ionosphere from an extreme space weather event. Overall, this September 9-10 dataset provides extraordinary signatures of major solar flare-induced ionospheric variability – from both strong M-class and historic X-class eruptions during high solar activity conditions.

Advancing modeling capabilities by incorporating such observational data would be invaluable for predicting the flare impacts on critical communications and navigation systems. The contrasting sub-tropical and equatorial ionospheric variability also offers excellent scope for targeted regional studies during dynamic space weather events in the future. With the approaching solar minimum, this current epoch of data collection constitutes an exceptional starting point to improve the understanding of ionospheric processes over the Indian subcontinent during extreme solar perturbations. Lei et al. (2018) analyzed the Total Electron Content (TEC) in the Asian Australian sector for the September 2017 event, revealing significant TEC enhancements during the recovery phase of the geomagnetic storm.

4. Conclusion

The occurrence of intense solar flare occurrences originating from active region AR2673 provided an invaluable opportunity to study space weather effects on the ionosphere. This paper investigated the total electron content (TEC) signatures of major X-class (X2.2, X9.3, X8.2) and M-class (M2.4, M7.3) solar flares alongside geomagnetic storms during September 6-11, 2017. Multiple locations from equatorial to high latitudes were covered. The distinct enhancements in TEC aligned with the flare timings affirm significant prompt penetration of disturbances from these solar eruptions that supplement ionization in the upper atmosphere. The TEC peaks were generally short-lived, recovering within 3-4 hours. However, TEC levels remained elevated for longer during intense activity. Significant differences were seen in sub-tropical and equatorial ionospheric responses in terms of TEC perturbation magnitudes and persistence. Equatorial regions registered TEC fluctuations up to twice as high as mid-latitudes due to added drivers like the pre-reversal enhancement and plasma instabilities. This highlights the demarcation in ionization processes and magnetic field configurations between the anomaly crest and polar regions. Comparison of the X9.3 disk flare and X8.2 limb flare evidenced the strong dependence of chromospheric EUV flux enhancement, and hence TEC variability, on the flare location relative to Earth. The ionospheric response signatures differed despite the comparable X-ray magnitudes of these events. Consideration of this solar-terrestrial geometry aspect is, therefore, essential for understanding and predicting ionospheric variability during solar storms.

Investigations into isolated flares occurring amid otherwise quiet geomagnetic conditions such as the X8.2 event enabled separating solar-induced effects. But during concurrent storms like on September 7-8, flares combined with other dynamic processes lead to TEC responses that require deconstruction through modeling. The presented observations constitute an effective database for advancing predictive capabilities tailored to this region. Overall, the September 6-11 episodes signify those solar flares can drastically impact the low-latitude ionosphere within minutes and induce hour-long disturbances – even overnight during events like the September 9 M1.1 flare. The intensity of TEC enhancements depends on the flare properties (class, duration, spectra) and background

conditions (time-of-day, geophysical state). The data provides unambiguous evidence of space weather effects propagating across terrestrial altitudes and longitudes, requiring extensive monitoring for mitigation. With solar activity expected to rise over the coming years, maintaining coverage through emerging ground and satellite assets is crucial. Detailed ionospheric quantification during this transitional era as exemplified in this study helps establish reference conditions for improving modeling and forecast systems specific to the Indian sector. As extreme events recur, the advancement of basic plasma physics processes in the upper atmosphere alongside a watchful ionosphere weather services framework will aid resilience against adverse impacts on relying technology a key necessity now recognized across sectors and policies.

In summary, this comprehensive analysis of ionospheric TEC variability demonstrates the enveloping but geographically non-uniform influence that powerful solar flares introduce across the coupled solar-terrestrial system. Tracking this energy transfer via key parameters like electron density enables deeper insight compared to relying on solar observations alone. The presented investigation techniques can serve as a template for future studies during the next active solar cycle in supporting improved space weather adaptation and preparedness.

5. Acknowledgments

Results presented in this paper rely on data collected at solar flare and Total electron Content (TEC) observatories so we thank national oceanic and atmospheric administration. (NOAA), Community coordinated modeling center (CCMC) – NASA and World.

ORCID iDs

Ashish Kumar Meena (https://orcid.org/0000-0002-1674-0252)
Preetam Singh Gour (https://orcid.org/0000-0003-1877-930X)

References

[1] Bagiya, M. S., Thampi, S. V., Hui, D., Sunil, A. S., Chakrabarty, D., & Choudhary, R. K. (2018). Signatures of the solar transient disturbances over the low latitude ionosphere from 6 to 8 September 2017. *Journal of Geophysical Research: Space Physics*, *123*(9), 7598-7608.

[2] Chakraborty, M., Singh, A. K., & Rao, S. S. (2021). Solar flares and geomagnetic storms of September 2017: Their impacts on the TEC over 75 E longitude sector. *Advances in Space Research*, *68*(4), 1825-1835.

[3] Chamberlin, P. C., Woods, T. N., Didkovsky, L., Eparvier, F. G., Jones, A. R., Machol, J. L., & Woodraska, D. L. (2018). Solar ultraviolet irradiance observations of the solar flares during the intense September 2017 storm period. *Space Weather*, *16*(10), 1470-1487.

[4] Coster, A., & Komjathy, A. (2008). Space weather and the global positioning system. *Space Weather*, *6*(6).

[5] Heelis, R. A., Lowell, J. K., & Spiro, R. W. (1982). A model of the high-latitude ionospheric convection pattern. *Journal of Geophysical Research: Space Physics*, *87*(A8), 6339-6345.

[6] Lei, J., Huang, F., Chen, X., Zhong, J., Ren, D., Wang, W., & Xue, X. (2018). Was magnetic storm the only driver of the long-duration enhancements of daytime total electron content in the Asian-Australian sector between 7 and 12 September 2017? *Journal of Geophysical Research: Space Physics*, *123*(4), 3217-3232.

[7] Li, N., Lei, J., Luan, X., Chen, J., Zhong, J., Wu, Q., & Lin, L. (2019). Responses of the D region ionosphere to solar flares revealed by MF radar measurements. *Journal of Atmospheric and Solar-Terrestrial Physics*, *182*, 211-216.

[8] Raparthi, M., Dodda, S. B., & Maruthi, S. (2023). Predictive Maintenance in IoT Devices using Time Series Analysis and Deep Learning. Dandao Xuebao/Journal of Ballistics, 35(3). https://doi.org/10.52783/dxjb.v35.113

[9] Liu, J. P., Li, A. C., Xu, K. H., Velozzi, D. M., Yang, Z. S., Milliman, J. D., & DeMaster, D. J. (2006). Sedimentary features of the Yangtze River-derived along-shelf clinoform deposit in the East China Sea. *Continental Shelf Research*, *26*(17-18), 2141-2156.

[10] Mitra, A. P. (1974). *Ionospheric effects of solar flares* (Vol. 46). Boston: Reidel.

[11] Pawlowski, D. J., & Ridley, A. J. (2008). Modeling the thermospheric response to solar flares. *Journal of Geophysical Research: Space Physics*, *113*(A10).

[12] Qian, L., Burns, A. G., Chamberlin, P. C., & Solomon, S. C. (2010). Flare location on the solar disk: Modeling the thermosphere and ionosphere response. *Journal of Geophysical Research: Space Physics*, *115*(A9).

[13] Qian, L., Burns, A. G., Chamberlin, P. C., & Solomon, S. C. (2011). Variability of thermosphere and ionosphere responses to solar flares. *Journal of Geophysical Research: Space Physics*, *116*(A10).

[14] Qian, L., Burns, A. G., Solomon, S. C., & Chamberlin, P. C. (2012). Solar flare impacts on ionospheric electrodynamics. *Geophysical Research Letters*, *39*(6).

[15] Qian, L., Wang, W., Burns, A. G., Chamberlin, P. C., Coster, A., Zhang, S. R., & Solomon, S. C. (2019). Solar flare and geomagnetic storm effects on the thermosphere and ionosphere during 6–11 September 2017. *Journal of Geophysical Research: Space Physics*, *124*(3), 2298-2311.

[16] Tsurutani, B. T., Judge, D. L., Guarnieri, F. L., Gangopadhyay, P., Jones, A. R., Nuttall, J., & Viereck, R. (2005). The October 28, 2003, extreme EUV solar flare and resultant extreme ionospheric effects: Comparison to other Halloween events and the Bastille Day event. *Geophysical Research Letters*, *32*(3).

[17] Yasyukevich, Y., Astafyeva, E., Padokhin, A., Ivanova, V., Syrovatskii, S., & Podlesnyi, A. (2018). The 6 September 2017 X-class solar flares and their impacts on the ionosphere, GNSS, and HF radio wave propagation. *Space Weather*, *16*(8), 1013-1027.

[18] Zhang, D., Xiao, Z., & Chang, Q. (2002). The correlation of flare's location on solar disc and the sudden increase of total electron content. *Chinese Science Bulletin*, *47*, 83-85.

[19] Zhang, R., Liu, L., Le, H., & Chen, Y. (2017). Equatorial ionospheric electrodynamics during solar flares. *Geophysical Research Letters*, *44*(10), 4558-4565.

[20] Meena, M. K., Meena, A. K., Gour, P. S. (2022). Analysis of coronal mass ejections and solar flares. *Int J Innovat Res Growth*, 11, 70-73.

[21] Vaswani, L. K., Gour, P. S., Meena, A. K., Soni, S. (2022). Geomagnetic storm in association with solar activities. *Int J Innovat Res Growth*, 11, 143-148.